

TOWARDS A CRACK PROPAGATION CRITERION AND DYNAMIC INSERTION OF COHESIVE ELEMENTS APPLIED TO THERMAL FATIGUE FAILURE OF COMETS/ASTEROIDS

D. Uribe ^{a,b}, P.-O. Bouchard ^a, D. Pino Muñoz ^a, M. Delbo ^b

^a MINES ParisTech, PSL Research University, CEMEF-Centre de mise en forme des matériaux, CNRS UMR 7635, CS 10207 rue Claude Daunesse, 06904 Sophia Antipolis Cedex, France, diego.uribe_suarez@mines-paristech.fr, pierre-olivier.bouchard@mines-paristech.fr, daniel.pino_munoz@mines-paristech.fr; ^b UNS-CNRS-Observatoire de la Cote d'Azur, marco.delbo@oca.eu

Mots-clés: Crack propagation, local stress field, energetic approach, cohesive zone models, dynamic insertion, remeshing techniques.

Abstract

One of the most challenging issues in computational fracture mechanics is the propagation of a crack through a finite element mesh for arbitrary crack paths. In this work, this is done based on an advanced remeshing technique. The crack direction is computed using the maximal circumferential stress criterion or the maximal strain energy release rate criterion. The propagation of the crack is achieved through the combination of an advanced remeshing technique that enables us to remesh over the computed direction, with dynamic insertion of cohesive elements in the remeshed zone and in a mesh-independent way, allowing in addition, fracture energy control. Finally, an application consisting in a well-known mixed-mode benchmark case is presented to show the robustness of this technique in terms of crack path.

1 Introduction

In the design of structures or machine components, it is crucial to identify the most likely mode of failure, as well as to be able to prevent catastrophic failures thanks to predictive damage and fracture criteria. Here lies the importance of fracture mechanics. A suited and proven approach for its study is the finite element method, even though, propagation of a crack through a finite element mesh for arbitrary crack paths is a challenging and demanding task [1]. To overcome this issue, crack propagation here is handled through the combination of an advanced remeshing technique [2] with dynamic insertion of cohesive elements [3] without dependence to the mesh. The last one allows the control of the energy released during the fracture process.

Fracture is not restricted just to engineering structures as we know it today, it also takes place in "natural objects" like rocks, the nuclei of comets and asteroids. It has been shown that temperature cycles on airless bodies of our Solar System can cause damaging of surface material eventually causing their failure and breakdown [4]. This damaging process, known as thermal cracking, consists in the nucleation and growth of micro-fractures inside the material due to the mechanical stresses induced by the diurnal/nocturnal temperature cycles. Thermal cracking of surface rocks, in addition to the impact of micrometeorites, can eventually lead to rocks' breakup and produce fresh "regolith". Regolith is the layer of unconsolidated material that covers planetary surfaces [5, 6]. Furthermore, it is proposed by several studies that also macroscopic fractures, mass-wasting, and material breakdown on asteroids and cometary nuclei could be explained as a consequence of thermal effects [7, 8]. For all the reasons above, thermal cracking is now considered a space (and Earth) weathering mechanism. Figure 1 shows some in situ images of fractures on the nucleus of 67P/Churyumov-Gerasimenko, those images were acquired by the CIVA cameras on-board PHILAE [9].

Even though the long-term goal of this project is to simulate crack propagation on asteroids/comets, for now this work will be focused on the fracture propagation mechanisms, which are still poorly understood in the case of space objects. The rest of the paper is organized as follows. In Section 2, the numerical method used here for crack propagation process is described; crack propagation criteria as well as important aspects of cohesive zone models are covered. Here it is also presented the novelty of this work, i.e., dynamic insertion of cohesive elements in a mesh independent way. Then a benchmark example is illustrated in Section 3 to show the accuracy of the proposed method calculating the crack propagation direction under mixed-mode loading. Finally some concluding remarks are presented in Section 4.

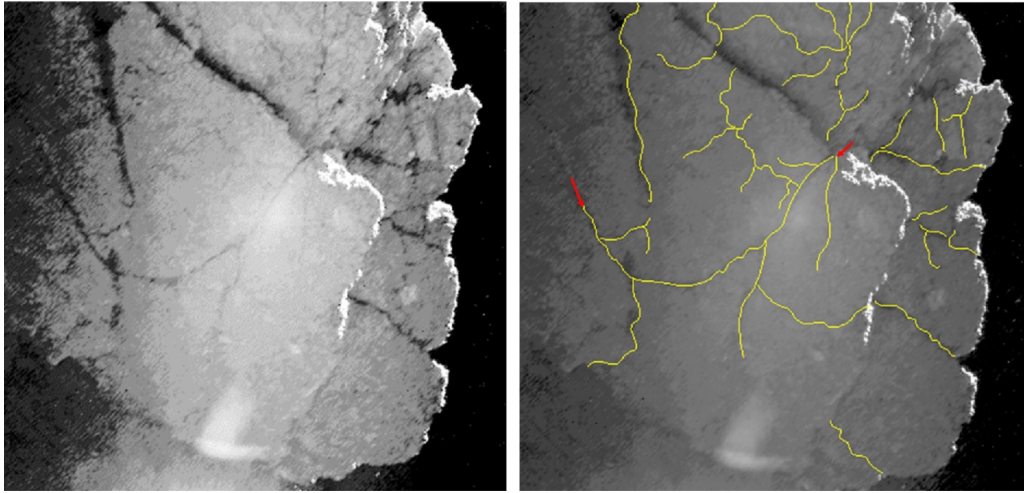


Figure 1: Fractured block observed in comet 67P/Churyumov-Gerasimenko nucleus. The left image was stretched to emphasize the fractures [9].

2 Crack Propagation

Once a crack has initiated, it is necessary to check if the crack is going to propagate or not, and in which direction. There are different criteria to find the direction of propagation of a crack, some criteria are based on the local fields at the crack tip, following a local approach, e.g. the maximum circumferential stress criterion [10]. Other criteria are based on the distribution of the energy throughout the cracked part like the maximal strain energy release rate criterion [11]. This work will cover the aforementioned criteria: The maximal circumferential stress criterion and the maximal strain energy release rate criterion.

2.1 Maximal circumferential stress criterion (MCSC)

This criterion proposed by Erdogan [10] states that a crack in an elastic material is going to propagate in the direction for which the circumferential stress ($\sigma_{\theta\theta}$) is maximum. This criterion is local because the direction of propagation is calculated using the stress field along a small circle of radius r centered at the crack tip (Figure 2). Through the solution of the following system it is possible to compute the kinking angle of the propagating crack:

$$K_I \sin(\theta) + K_{II} (3 \cos(\theta) - 1) = 0 \quad \text{with} \quad \begin{cases} K_I \sin(\frac{\theta}{2}) < 0 \\ \theta \in [-\pi, \pi] \\ K_I > 0 \end{cases} \quad (1)$$

where K_I and K_{II} correspond respectively to the stress intensity factors for mode I and II, and θ is the kinking angle. According to this criterion there is a limit angle corresponding to pure shear: $\theta = \pm 70.54^\circ$ [10].

The stress intensity factors (K_I and K_{II}) may be calculated through the finite element method, if not, the angle has to be computed based on the circumferential stress $\sigma_{\theta\theta}$ at each integration point of each one of the elements attached to the crack tip (Figure 3). Then the crack propagation is performed towards the integration point that maximises $\sigma_{\theta\theta}$. In Figure 2 it is shown the way a stress tensor of an element located at a distance r from the crack tip and defined in a cartesian coordinate system ($x - y$) should be rotated an angle θ to find the stress in the θ direction ($\sigma_{\theta\theta}$).

In this work we use a mixed finite element formulation with first-order elements using linear interpolation functions for both velocity and pressure ($P1 + /P1$). These P1 elements are not very good at capturing the singularity of the stress field at the crack tip (a huge mesh refinement would be necessary). The accuracy of the stress field would require the use of quadratic elements or of special elements such as the Barsoum (or quarter point) element [12] which accounts for the stress singularity. Without those elements, the use of an energetic approach may be more appropriate.

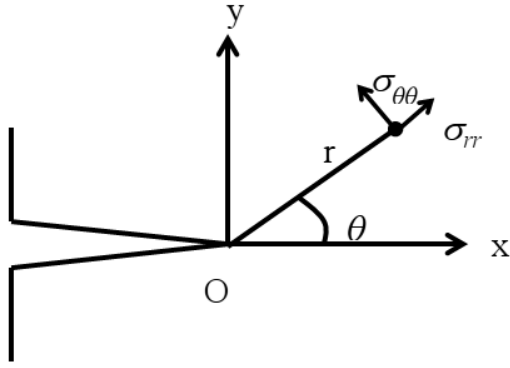
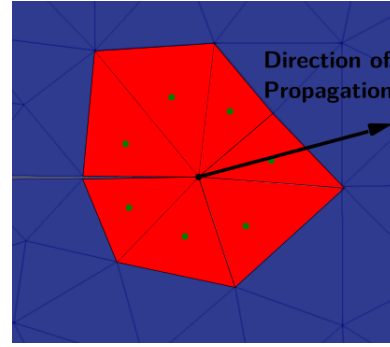
Figure 2: Criterion of Maximum $\sigma_{\theta\theta}$ 

Figure 3: Elements attached to the crack tip

2.1.1 Maximal strain energy release rate criterion (MSERRC)

According to this criterion the direction of propagation of a crack will be the one which maximises the strain energy release rate, i.e., the energy required to increase the crack length by one unity. It is evaluated using all virtual and kinematically admissible displacement field at the crack tip neighborhood. The direction of crack propagation can be determined by:

$$\begin{cases} \left(\frac{dG}{d\theta}\right)_{\theta=\theta_0} = 0 \\ \left(\frac{d^2G}{d\theta^2}\right)_{\theta=\theta_0} \leq 0 \end{cases} \quad (2)$$

Where θ_0 corresponds to the direction of propagation. Here for the computation of the strain energy release rate (G), the numerical technique known as $G\theta$ method [13] will be used. This method is based on a virtual displacement field V . According to Bouchard et al. [14] the $G\theta$ method is very accurate and completely mesh independent. Additionally, its implementation is quite simple and multiple extensions are available. Those are the principal reasons that encourages us in the present work to use this method. In the implementation of the $G\theta$ method adopted here, we first defined two contours C_1 and C_2 around the crack tip, those contours divide this region into three domains (Figure 4-a). Then it is defined a virtual displacement field $V(v_1, v_2)$ as the one shown in equation (3):

$$\begin{cases} v_1 = \left(1 - \frac{IM}{IJ}\right) \cos(\theta) \\ v_2 = \left(1 - \frac{IM}{IJ}\right) \sin(\theta) \end{cases} \quad (3)$$

Finally using equation (4) well described in [14], the energy release rate is calculated for the ring of elements for a given angle θ belonging to $[-70^\circ, 70^\circ]$ [10]. The $G\theta$ method provides an efficient way of computing G for a virtual extension in the direction θ .

$$G = \int_{ring} \left(Tr(\sigma \nabla U \nabla V) - \frac{1}{2} Tr(\sigma \nabla U) \nabla \cdot V \right) dC \quad (4)$$

Where σ and ∇U are respectively, the stress tensor and the gradient of the displacement, both coming from the finite element simulation, and ∇V is the gradient of the virtual displacement field. In Figure 4-a, it is considered a virtual ring and it is accounted for all the integration points belonging to this virtual ring. At the end a list of G values for each θ will be had, so it should be found the maximum (Figure 4-b), and the direction of propagation will be the value of θ that corresponds with the maximum value of G , i.e., the maximum of the curve $G(\theta)$ in Figure 4-b.

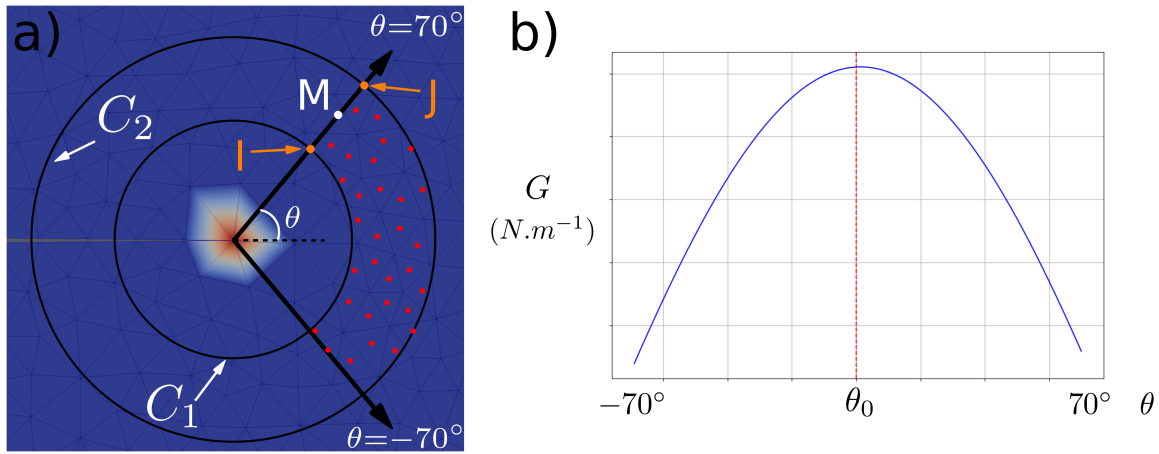


Figure 4: **a)** Ring of elements around the crack tip with the contours and domains used to computed G through the $G\theta$ method. **b)** $G(\theta)$ curve.

2.2 Mesh Independent Cohesive Zone Models

A pioneer perspective stating that fracture is a phenomenon taking place across an extended crack tip (cohesive zone), was proposed back in the 60's [15, 16]. The proposed concept was named as cohesive zone models (CZM), a simple approach asserting that at the crack tip, there is a finite size region where there is a transition from a fully broken material to a sound material [17]. In Figure 5 it is shown a schematic representation of the cohesive region, also known as process zone, where fracturing process is taking place in a brittle material. Cohesive zone corresponds to prospective fracture surfaces ahead of a crack which are permitted to separate under loading. Atomic or molecular forces are in charge of preventing the process of separation and creation of crack surfaces [18]. The force that exerts resistance to the opening of the new surfaces is known as cohesive force, and it is modeled through a phenomenological traction-separation law (cohesive law). It does not exist just one cohesive law used to model the fracture process, many of them can be used. In Figure 6 it is depicted the irreversible exponential cohesive law used in this work.

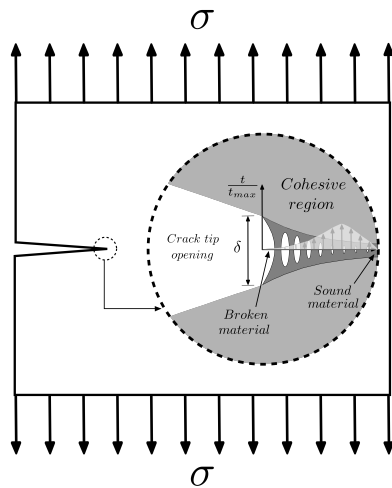


Figure 5: Schematic representation of the cohesive zone.

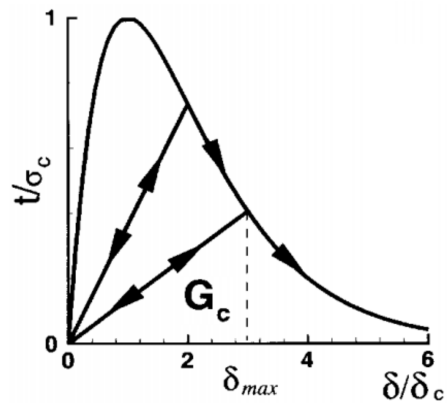


Figure 6: Cohesive law in terms of an effective opening displacement δ and traction t (loading-unloading envelop) [3].

The irreversibility characteristic is manifested once upon unloading. The critical energy release rate G_c , i.e. the fracture energy required to create the new free surfaces and break the material, and the cohesive law can be related in the following way:

$$G_c = \int_0^\infty t d\delta \tag{5}$$

Where t is a scalar effective traction and δ is an effective opening displacement. Equation 5 represents the control of the fracture energy that cohesive zone models allow us to have during the fracture process. The control of the fracture energy given by this methodology is one of the reasons that highly encourages the use of the cohesive zone models (cohesive elements) in our work. Commonly, cohesive zone models have been used to solve problems involving interfaces, surfaces undergoing decohesion or problems where the crack path is known a priori [19, 20]. Once the direction of propagation (blue dashed line in Figure 7-a) is computed using one of the already described criteria, Figure 7-b shows the procedure that has been widely used in the literature to insert cohesive elements. These are inserted through the closer edges and nodes to the computed direction. Figure 7-c shows the methodology used here, where before inserting the cohesive elements, a remeshing procedure over the predicted direction is performed [2]. In this way, it is assured that the crack path is not going to be a good approximation of the computed one, instead it is going to be exact.

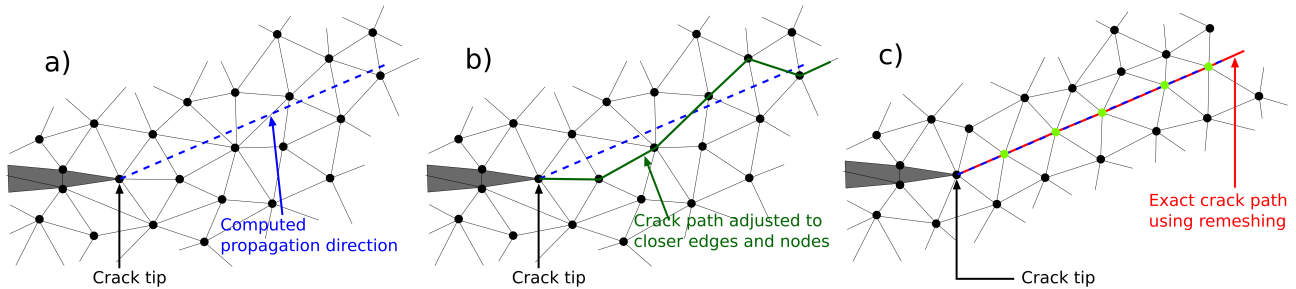


Figure 7: **a)** Prescribed crack path (dashed blue line). **b)** Insertion process of cohesive elements previously used in literature. **c)** Insertion process of cohesive elements used in this work.

The insertion of cohesive elements in the way showed in Figure 7-b exhibits a mesh dependency behaviour, so if the mesh changes, the crack pattern slightly changes too [21]. Conversely the process showed in Figure 7-c is mesh-independent. Inserting cohesive elements **on the fly**, i.e., while the crack tip is propagating through the domain, avoids a well known strong drawback in the implementation of cohesive zone models into a FE framework: artificial reduction of the stiffness of the material (modification of the global stiffness of the material). Other implications regarding how cohesive elements can be used to model fracture are well discussed in [21]. When remeshing has been performed, the insertion process of cohesive elements can take place. A graphical illustration of the insertion process done in this work is shown in Figure 8. Pragmatically, two neighbor bulk elements are separated by inserting a cohesive element at their shared face. This insertion is carried out by just duplicating the nodes forming the separating face and inserting a new cohesive element linking the original nodes to the new duplicated ones (Figure 8-c). In part **a** it can be seen the red dashed line showing the faces that will be split. **b** shows the blue dots corresponding to the nodes that have been doubled (indeed there are two nodes at the same location). The red line corresponds to a initially flat cohesive element. And finally in **c** it can be seen that after loading, the new inserted cohesive elements open.

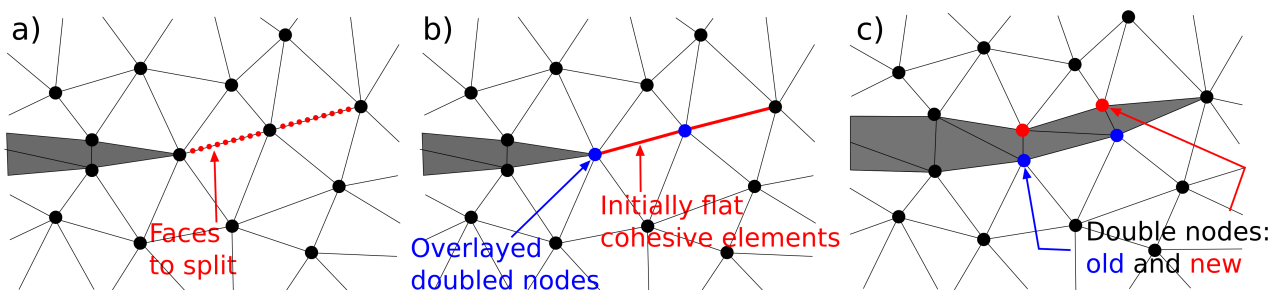


Figure 8: Schematic representation of the insertion of cohesive elements.

3 Results

The maximum circumferential stress criterion and the maximum strain energy release rate criterion (using the $G\theta$ method) have been implemented in our inhouse library and tests have been performed. Figure 9 shows the benchmark case tested in this work.

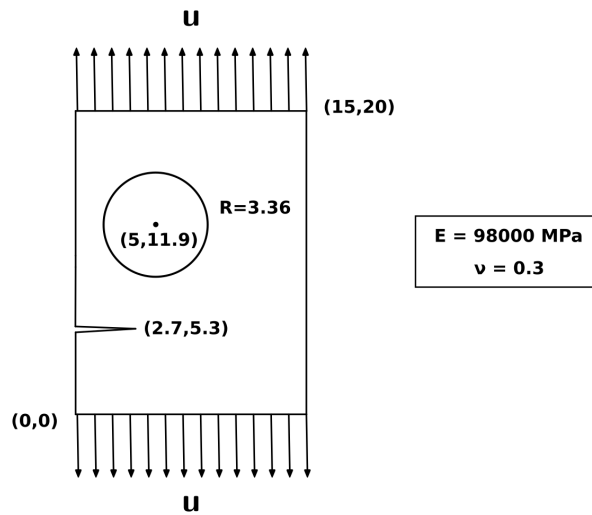


Figure 9: Single edge crack with off-centre hole (units in *mm*)

For the proposed benchmark case it will be shown the results regarding first, the insertion of cohesive elements after remeshing operations and crack propagation, second the crack path for the proposed geometry under the given loading configurations (mixed-mode), and finally it will be shown a comparison of the computed crack path using the maximum circumferential stress criterion and the maximum strain energy release rate criterion. For the sake of simplicity, in the example developed in this paper, the crack growth distance is set to a fixed value equal to 3 times the element size of the mesh.

3.1 Cohesive elements insertion

Figure 10-a shows the crack tip position at time step n , it is also shown a red line depicting the computed crack propagation direction. Figure 10-b shows the crack tip position after propagation at time step $n + 1$, it also shows a dashed magenta line illustrating the performed remeshing operation and the previous crack tip position. Finally Figure 10-c shows a zoom detail of the inserted cohesive elements (red) along the crack path.

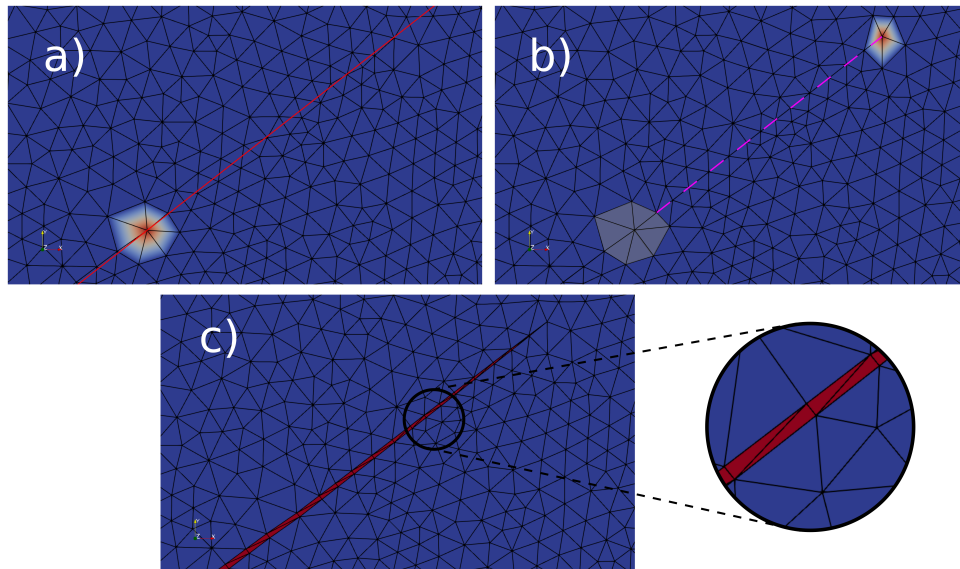


Figure 10: **a)** Crack tip position time step n . **b)** Crack tip position time step $n + 1$. **c)** Inserted cohesive elements

3.2 Crack path

Figure 11-a shows the crack propagation for a single edge crack with off-centre hole. According to [22] and [1], under this configuration the propagation of the crack should be affected by the presence of the off-centre hole, effect that is observed in the results. The crack at the start is attracted by the hole, and after passing the

hole, the crack continues propagating horizontally. Figure 11-b shows the performed comparison between the results obtained from the MCSC and the MSERRC. The crack path computed using MSERRC is smoother than the one obtained from MCSC. This can be due to the fact that MCSC is sensitive to the local stress field at the immediate crack tip. $P1 + /P1$ elements are not accurate enough to capture the stress singularity correctly which can lead to such oscillations. With the MSERRC, the strain energy release rate computation is carried out in a ring of elements further from the crack tip, in an area with lower stress gradients, which makes this method more accurate.

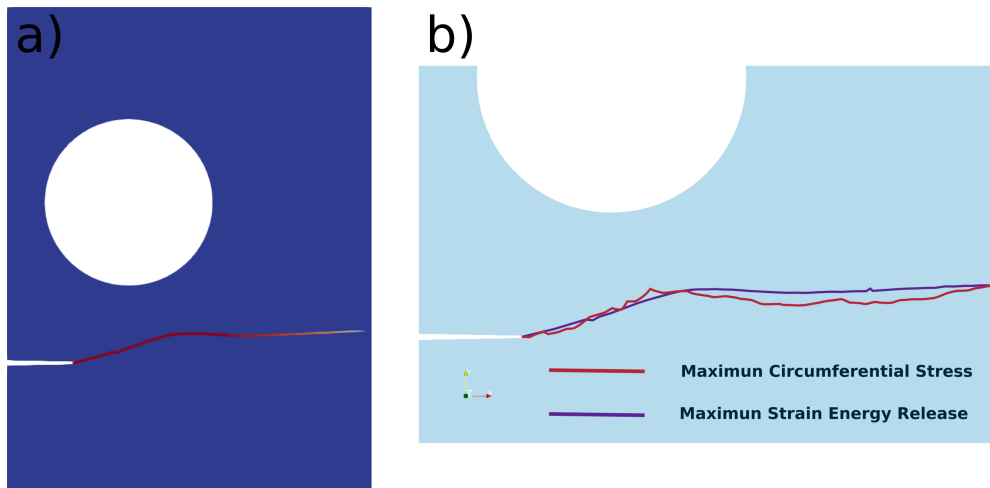


Figure 11: A) Crack path of a single edge crack with off-centre hole. B) Comparison between MCSC and the MSERRC.

4 Conclusions

In the previous section it was presented the preliminary results obtained for crack propagation under mixed-mode loading in brittle materials. This was done through the combination of an advanced remeshing technique that enables remeshing over the exact computed direction, with dynamic insertion of cohesive elements in the remeshed zone, allowing in addition the control of the energy released due to the fracture process. Combination of the aforementioned methodologies is the biggest novelty here. An energetic approach allowed to calculate in an appropriate way the crack propagation direction. The work presented here is immersed in a new approach that allows the crack propagation using remeshing operations and cohesive elements in a mesh-independent way. Even though the results obtained here are promising, there are still several studies that have to be carried out: the effect of the different cohesive parameters on the crack path should be studied, this approach has to be applied to thermal cracking, the developed scheme should be extended to multiple cracks and of course, it also has to be extended to 3D.

Acknowledgements

We acknowledge support from Academies of Excellence on Complex Systems and Space, Environment, Risk and Resilience of the Initiative d'EXcellence "Joint, Excellent, and Dynamic Initiative" (IDEX JEDI) of the Université Côte d'Azur and the Center for Planetary Origin (C4PO) A Material approach (<https://www-n.oca.eu/morby/C4PO/C4PO-home.html>). We also acknowledge support from The DIGIMU ANR industrial chair (<https://chaire-digimu.cemef.mines-paristech.fr/>).

References

- [1] P.-O. Bouchard, F. Bay, Y. Chastel, and I. Tovena. Crack propagation modelling using an advanced remeshing technique. *Computer Methods in Applied Mechanics and Engineering*, 189(3):723 – 742, 2000.
- [2] M. Shakoor, M. Bernacki, and P.-O. Bouchard. A new body-fitted immersed volume method for the modeling of ductile fracture at the microscale: Analysis of void clusters and stress state effects on coalescence. *Engineering Fracture Mechanics*, 147:398 – 417, 2015.

- [3] M. Ortiz and A. Pandolfi. Finite-deformation irreversible cohesive elements for three-dimensional crack-propagation analysis. *Int J Numer Methods Eng*, 1999.
- [4] M. Delbo, G. Libourel, J. Wilkerson, N. Murdoch, P. Michel, K. T. Ramesh, C. Ganino, C. Verati, and S. Marchi. Thermal fatigue as the origin of regolith on small asteroids. *Nature*, 508(7495):233–236, 2014.
- [5] J. Veverka, P. C. Thomas, M. Robinson, S. Murchie, C. Chapman, M. Bell, A. Harch, W. J. Merline, J. F. Bell, et al. Imaging of small-scale features on 433 eros from near: Evidence for a complex regolith. *Science*, 292(5516):484–488, 2001.
- [6] N. Murdoch, P. Sánchez, S. R. Schwartz, and H. Miyamoto. *Asteroid Surface Geophysics*, pages 767–792. 2015.
- [7] M. El Maarry, N. Thomas, A. Gracia Berná, R. Marschall, A. Auger, O. Groussin, S. Mottola, M. Pajola, M. Massironi, et al. Fractures on comet 67p/churyumov-gerasimenko observed by rosetta/osiris. *Geophysical Research Letters*, 42(13):5170–5178, 2.
- [8] V. Alf-Lagoa, M. Delbo, and G. Libourel. Rapid temperature changes and the early activity on comet 67p/churyumov-gerasimenko. *The Astrophysical Journal Letters*, 810(2):L22, 2015.
- [9] F. Poulet, A. Lucchetti, J.-P. Bibring, J. Carter, B. Gondet, L. Jorda, Y. Langevin, C. Pilorget, C. Capanna, and G. Cremonese. Origin of the local structures at the Philae landing site and possible implications on the formation and evolution of 67P/Churyumov-Gerasimenko. *Monthly Notices of the Royal Astronomical Society*, 462(Suppl1): S23–S32, 2016.
- [10] F. Erdogan and G. C. Sih. On the crack extension in plates under plane loading and transverse shear. *Journal of Basic Engineering*, 85(4):519–525, 1963.
- [11] M. Hussain, S. Pu, and J. Underwood. *Strain Energy Release Rate for a Crack Under Combined Mode I and Mode II. Fracture Analysis, Proc. 1973 National Symposium on Fracture Mechanics, Part II, ASTM STP 560, Amer. Soc. Testing Mater*, pages 2–28, 1973.
- [12] R. S. Barsoum. On the use of isoparametric finite elements in linear fracture mechanics. *International Journal for Numerical Methods in Engineering*, 10(1):25–37, 1976.
- [13] P. Destuynder, M. Djaoua, and S. Lescure. Quelques remarques sur la mécanique de la rupture élastique. *J. Méca. Théo. Appl.*, 2(1):113–135, 1983.
- [14] P.-O. Bouchard, F. Bay, and Y. Chastel. Numerical modelling of crack propagation: automatic remeshing and comparison of different criteria. *Computer Methods in Applied Mechanics and Engineering*, 192(35):3887 – 3908, 2003.
- [15] G. I. Barenblatt. The mathematical theory of equilibrium cracks in brittle fracture. In H. L. Dryden, T. von Kármán, G. Kuerti, F. H. van den Dungen, and L. Howarth, editors, *Advances in Applied Mechanics*, volume 7, pages 55–129. Elsevier, 1962.
- [16] J. R. Rice. A path independent integral and the approximate analysis of strain concentration by notches and cracks. *Journal of Applied Mechanics*, 35(2):379–386, 1968.
- [17] D. S. Dugdale. Yielding of steel sheets containing slits. *Journal of the Mechanics and Physics of Solids*, 8(2):100–104, 1960.
- [18] J. R. Rice. Mathematical analysis in the mechanics of fracture. In H. Liebowitz, editor, *Fracture : an advanced treatise.*, chapter 3, pages 191–311. Academic Press, N.Y., 1968.
- [19] M. Alfano, F. Furguele, A. Leonardi, C. Maletta, and G. H. Paulino. Cohesive zone modeling of mode i fracture in adhesive bonded joints. In *Advances in Fracture and Damage Mechanics VI*, volume 348 of *Key Engineering Materials*, pages 13–16. Trans Tech Publications, 7 2007.
- [20] A. Turon, P. Camanho, J. Costa, and J. Renart. Accurate simulation of delamination growth under mixed-mode loading using cohesive elements: Definition of interlaminar strengths and elastic stiffness. *Composite Structures*, 92(8):1857 – 1864, 2010.
- [21] M. Shakoor, V. T. Navas, D. P. Muñoz, M. Bernacki, and P.-O. Bouchard. Computational methods for ductile fracture modeling at the microscale. *Archives of Computational Methods in Engineering*, pages 1–40, 2018.
- [22] M. Rashid. The arbitrary local mesh replacement method: An alternative to remeshing for crack propagation analysis. *Computer Methods in Applied Mechanics and Engineering*, 154(1):133 – 150, 1998.